Available online at www.sciencedirect.com
ScienceDirect
Communications in Nonlinear Science and Numerical Simulation 13 (2008) 81–87
Communications in Nonlinear Science and Numerical Simulation
www.elsevier.com/locate/cnsns

Computing ITG turbulence with a full-*f* semi-Lagrangian code

V. Grandgirard [a,*], Y. Sarazin [a], X. Garbet [a], G. Dif-Pradalier [a], Ph. Ghendrih [a], N. Crouseilles [b], G. Latu [b], E. Sonnendrücker [b], N. Besse [c], P. Bertrand [c]

[a] *Association Euratom-CEA, CEA/DSM/DRFC, CEA-Cadarache, France*
[b] *IRMA, Université Louis Pasteur, 7, rue René Descartes, 67084 Strasbourg Cedex, France*
[c] *LPMIA, Université Henri Poincaré-Nancy 1, BP 239, 54506 Vandoeuvre-les-Nancy, France*

Available online 25 May 2007

Abstract

This paper addresses non-linear global gyrokinetic simulations of ion temperature gradient (ITG) driven turbulence with the GYSELA code. The particularity of GYSELA code is to use a semi-Lagrangian (SL) scheme for the full distribution function. The 4D non-linear drift-kinetic version of the code already shows the interest in such a SL method which exhibits good properties of energy conservation. The code has been upgrated to run 5D toroidal simulations. Linear benchmarks and non-linear results are presented.

PACS: 52.30.Gz

Keywords: Gyrokinetic; Semi-Lagrangian; Ion-temperature-gradient; Plasma turbulence

1. Introduction

Non-linear gyrokinetic simulations are playing an increasingly important role in understanding anomalous transport in magnetically confined fusion plasmas. In spite of considerable progress, the choice of the method for solving the Vlasov equation is still in debate. The most widespread method is the Lagrangian scheme (typically particle-in-cell codes). An alternative is the Eulerian method. These two approaches have already proved their efficiency. However the fact that the PIC simulations can be affected by numerical noise is a subject of controversy [1]. Techniques of "optimal loading" [2] and filtering have been recently developed to improve this problem. Regarding the Eulerian codes they require numerical schemes of high order to limit numerical dissipation. This paper deals with gyrokinetic simulations performed with a new method based on a semi-Lagrangian (SL) scheme [3]. In the GYSELA code the full distribution function is evolved on a fixed grid in the phase space, moving backwards in time along the characteristics. A 4D drift-kinetic slab-ITG version of the code has already shown good properties of energy conservation in non-linear regime as well as an

* Corresponding author. Tel.: +33 4 42 25 61 19; fax: +33 4 42 25 49 90.
E-mail address: virginie.grandgirard@cea.fr (V. Grandgirard).

1007-5704/$ - see front matter
doi:10.1016/j.cnsns.2007.05.016

accurate description of fine spatial scales [4,5]. The first results obtained with the new 5D gyrokinetic toroidal version of GYSELA are presented.

2. A gyrokinetic 5D model in toroidal geometry

The model focuses on the turbulent transport driven by the collisionless ITG instability in a simple toroidal geometry (the magnetic flux surfaces are taken to be concentric torii with circular poloidal cross-sections). Since the turbulence frequency ω is much smaller than the ion cyclotron frequency $\omega_c = \frac{e_i B_0}{m_i}$ ($e_i = Z_i e$ is the ion charge and m_i the ion mass), the gyrokinetic description is appropriate. The magnetic configuration is a circular concentric tokamak configuration: $\boldsymbol{B} = (B_0 R_0/R)\boldsymbol{b}$ with the unit vector $\boldsymbol{b} = (1/\sqrt{1+(r/qR)^2})(\boldsymbol{e}_\varphi + (r/qR)\boldsymbol{e}_\theta)$. B_0 and R_0 correspond to the magnetic field and the major radius of the torus computed at the magnetic axis, with $R = R_0 + r\cos\theta$. $\boldsymbol{e}_\theta$ and $\boldsymbol{e}_\varphi$ are the unit vectors in the two periodic directions, poloidal and toroidal respectively. The safety factor profile $q(r) = \boldsymbol{B}\cdot\nabla\varphi/\boldsymbol{B}\cdot\nabla\theta$ is defined by the three parameters q_0, δ_q, and α_q such that $q(r) = q_0 + \delta_q (r/a)^{\alpha_q}$. The fluctuations of the magnetic field are neglected. Thus the electrostatic approximation is used to compute the electric field, i.e. $\boldsymbol{E} = -\nabla\phi$, where the scalar ϕ represents the electric potential. Electrons are assumed adiabatic, so that $\delta n_e/n_0 = e(\phi - \langle\phi\rangle)/T_e$, where n_0 is the equilibrium particle density profile. The brackets $\langle\cdot\rangle$ refer to the magnetic flux surface average. Taking into account the velocity drifts up to the first order in $\omega/\omega_c \ll 1$ and in the limit $\varepsilon = r/R \ll 1$, the trajectories of the ion guiding-centers are governed by:

$$\frac{\mathrm{d}r}{\mathrm{d}t} = v_{\bar{E}r} + v_{g_r}; \quad \frac{\mathrm{d}\theta}{\mathrm{d}t} = \frac{v_\parallel}{q(r)R} + \frac{1}{r}(v_{\bar{E}\theta} + v_{g\theta}); \quad \frac{\mathrm{d}\varphi}{\mathrm{d}t} = \frac{v_\parallel}{R} \tag{1}$$

$$\frac{\mathrm{d}v_\parallel}{\mathrm{d}t} = -\frac{e_i}{m_i}\nabla_\parallel\bar{\phi} - \frac{\mu}{m_i}\nabla_\parallel B + \frac{v_\parallel}{B}(\boldsymbol{v}_E\cdot\nabla B) \quad \text{with} \quad \nabla_\parallel = \frac{1}{R}\left[\partial_\varphi + \frac{1}{q(r)}\partial_\theta\right] \tag{2}$$

$v_\parallel$ is the velocity parallel to the magnetic field. The magnetic moment $\mu = m_i v_\perp^2/(2B)$ is an adiabatic invariant with $v_\perp$ the velocity in the plane orthogonal to the magnetic field. The subscripts r and θ refer to the radial and poloidal components, respectively. The electric drift velocity $v_{\bar{E}}$ is computed with the gyro-average of the electric potential $\bar{\phi}$: $\boldsymbol{v}_{\bar{E}} = (\boldsymbol{B}\times\nabla\bar{\phi})/B^2$. At low β, the curvature drift velocity $\boldsymbol{v}_{g\perp}$ is given by $\boldsymbol{v}_{g\perp} = \left(\frac{\boldsymbol{B}}{eB^2}\times\frac{\nabla B}{B}\right)(m_i v_\parallel^2 + \mu B)$ which reads, in the large aspect ratio limit, $\boldsymbol{v}_{g\perp} = v_g[\sin\theta\boldsymbol{e}_r + \cos\theta\boldsymbol{e}_\theta]$ with $v_g = -(m_i v_\parallel^2 + \mu B)/(eB_0R_0)$. The time evolution of the guiding-center 5D distribution function $\bar{f}(r,\theta,\varphi,v_\parallel,\mu,t)$ is governed by the Vlasov equation averaged over the cyclotron motion (so-called gyrokinetic equation):

$$\frac{\partial\bar{f}}{\partial t} + \frac{\mathrm{d}r}{\mathrm{d}t}\frac{\partial\bar{f}}{\partial r} + \frac{\mathrm{d}\theta}{\mathrm{d}t}\frac{\partial\bar{f}}{\partial\theta} + \frac{\mathrm{d}\varphi}{\mathrm{d}t}\frac{\partial\bar{f}}{\partial\varphi} + \frac{\mathrm{d}v_\parallel}{\mathrm{d}t}\frac{\partial\bar{f}}{\partial v_\parallel} = 0 \tag{3}$$

In that form, $\bar{f}$ is clearly constant along the characteristics (2). The electric quasi-neutrality provides the self-consistency condition of the problem. Using the notation $\nabla_\perp = (\partial_r, \frac{1}{r}\partial_\theta)$, it reads:

$$-\frac{1}{n_0(r)}\nabla_\perp\cdot\left[\frac{n_0(r)}{B_0\omega_c}\nabla_\perp\phi\right] + \frac{e}{T_e(r)}[\phi - \langle\phi\rangle] = \frac{1}{n_0(r)}\left[n_{\mathrm{Gi}}(r,\theta,\varphi) - n_{\mathrm{Gi}_{\mathrm{eq}}}(r,\theta)\right] \tag{4}$$

where n_{Gi} is the ion guiding-center density given by $n_{\mathrm{Gi}} = 2\pi\int B/m_i\,\mathrm{d}\mu\int\mathrm{d}v_\parallel J_0(k_\perp\rho_c)\cdot\bar{f}$, ρ_c being the Larmor radius. The first term on the left hand side is known as the polarization term which corresponds to the difference between the guiding-center density and that of particles. The correction term $n_{\mathrm{Gi}_{\mathrm{eq}}}$ is equal to $n_{\mathrm{Gi}_{\mathrm{eq}}} = 2\pi\int B/m_i\,\mathrm{d}\mu\int\mathrm{d}v_\parallel J_0(k_\perp\rho_c)\cdot\bar{f}_{\mathrm{eq}}$. The Bessel function J_0, corresponds to the gyro-average operator in Fourier space. The discretization of this quasi-neutrality equation (4) is performed by projecting in Fourier space along the two periodic directions (θ and φ) and by using finite differences in the radial direction.

3. Choice of an equilibrium depending on the motion invariants only

The radial profiles of the ion temperature and of the density (respectively $T_i(r)$ and $n_0(r)$) are fixed in time and deduced by numerical integration of their gradient profiles given by the two parameters κ and

$\Delta r : \mathrm{d}\log T_i(r)/\mathrm{d}r = -\kappa_{T_i}\cosh^{-2}((r-r_p)/\Delta r_{T_i})$ with r_p corresponding to the middle of the radial box. The distribution function is periodic along θ and φ. Vanishing perturbations are imposed at the boundaries in the non-periodic directions, namely r and $v_\parallel$. Such boundary conditions may be subject to numerical instabilities if turbulence spreads up to the radial borders. In this case, buffer regions with overdamped fluctuations should be incorporated. Initial conditions consist of an equilibrium distribution function $\bar{f}_{\mathrm{eq}}$ perturbed by a sum of accessible (m,n) Fourier modes (m and n being the poloidal and toroidal wave numbers, respectively). Previously the equilibrium distribution function was chosen equal to a conventional Maxwellian distribution function:

$$\bar{f}_{\mathrm{eq}} = f_{\mathrm{M}}(r,E) = n_0(r) \times [2\pi T_i(r)/m_i]^{-\frac{3}{2}} \exp(-E/T_i(r)) \tag{5}$$

with $E = \frac{1}{2}m_i v_\parallel^2 + \mu B(r,\theta)$, the energy, which is the second invariant of the system. But it appears that it is crucial to choose $\bar{f}_{\mathrm{eq}}$ to be a function of the motion invariants, especially for studying zonal flows. Indeed, breaking this rule leads to the development of large scale steady flows, which prevent the onset of turbulence (see following non-linear results), consistently with previous observations [6,7]. Due to the axisymetric magnetic topology, the third motion invariant is the toroidal kinetic moment P_φ; $P_\varphi = e_i\Psi + m_i R v_\varphi$, Ψ being the toroidal magnetic flux. As a consequence, the equilibrium distribution function can be initialized to a canonical Maxwellian, as in (5), but where the radius r is replaced by the motion invariant $\bar{r}$ defined as [7]:

$$\bar{r} = r_p - \frac{q_p}{r_p}[\psi(r) - \psi(r_p)] - \frac{mq_p}{eB_0 r_p}[Rv_\parallel - R_0\bar{v}_\parallel] \tag{6}$$

where $\psi(r) = -B_0\int_0^r \frac{r'\mathrm{d}r'}{q}$. The expression of $\bar{v}_\parallel = \mathrm{sign}(v_\parallel)\sqrt{2/m}\sqrt{E-\mu B_{\max}}H(E-\mu B_{\max})$ has been chosen to minimize poloidal flows (cf. [8]). With this expression the difference between $\bar{r}$ and r is of order $\rho_* = \rho_i/a$, ρ_i is the ion Larmor radius and a the minor radius.

4. Linear benchmark with the classical cyclone DIII-D case

The numerical solution is computed using normalized equations. In our case, the temperature is normalized to $T_{\mathrm{e}0}$, where $T_{\mathrm{e}0}$ is defined by the initial temperature profile such that $T_{\mathrm{e}}(r_p)/T_{\mathrm{e}0} = 1$. The time is normalized to the inverse of the ion cyclotron frequency $\omega_{\mathrm{c}} = e_i B_0/m_i$. Velocities, including the parallel velocity, are expressed in units of the ion speed $v_{T0} = \sqrt{T_{\mathrm{e}0}/m_i}$, the electric potential is normalized to $T_{\mathrm{e}0}/e_i$ and the magnetic field is normalized to B_0. Consequently, lengths are normalized to the Larmor radius $\rho_s = m_i v_{T0}/e_i B_0$ and the magnetic moment μ to $T_{\mathrm{e}0}/B_0$. In this section, we show the results of the benchmark test with the cyclone base case [9]. The standard dimensionless parameters are: $R_0/L_T = 6.92$, $R_0/L_n = 2.2$, $\varepsilon = a/R_0 = 0.18$, $q = 1.4$, $s \equiv (r/q)(\mathrm{d}q/\mathrm{d}r) = 0.8$, $\rho_* = 1/184.7$ and $T_{\mathrm{e}}/T_i = 1$ where L_T and L_n are the temperature and density gradient scale lengths, respectively. The difficulty with a global full-f code as GYSELA is that these Cyclone parameters can only be satisfied locally. Besides, as the equilibrium distribution function is not initialized by a classical Maxwellian, the profiles, that really play a role in the simulation, are not n_0 and T_i but $n_{\mathrm{eq}}(r) = \int J_0 f_{\mathrm{eq}}\,\mathrm{d}\theta d_3 v$ for the density and $T_{i\,\mathrm{eq}}(r) = \int J_0 f_{\mathrm{eq}} E\,\mathrm{d}\theta d_3 v/n_{\mathrm{eq}}(r)$ for the temperature. The correction

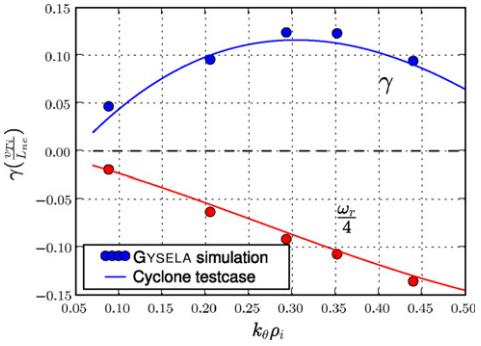

Fig. 1. Linear mode growth rates and frequencies versus $k_\theta\rho_i$ for the Cyclone DIII-D base case. The GYSELA results are plotted with circle points. The solid line represents a linear interpolation of all the results presented in paper [9].

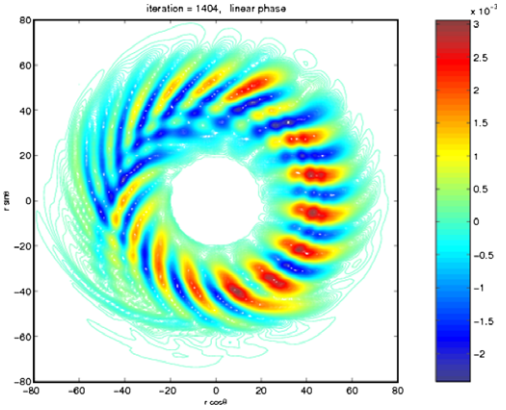

Fig. 2. Poloidal cross-section of the electric potential for the most unstable mode $(m,n) = (10,-14)$.

is a correction of order ρ_* that is such that the contribution at a given position r depends on the contribution at various values of $\bar{r}$ due to the velocity dependence of the latter coordinate. The effective gradients that are relevant depart from the values selected for the initial conditions. For this reason the cyclone test has been performed by first calibrating the required profiles to recover the growth rate and the frequency of the most unstable mode $(m,n) = (10,-14)$ (see its ballooning mode structure in Fig. 2). The corresponding parameters are the following $\kappa_n = 2.2$, $\Delta_{r_n} = 5$, $\kappa_T = 6.78$, $\Delta_{r_T} = 0.8$ with $\rho_* = 0.01$. Then the same parameters have been used to perform the four others simulations for $(m,n) = (4,-3),(7,-10),(12,-17)$ and $(21,-15)$. For these five simulations the radial domain is limited to the region of $0.2 < r/a < 0.8$. (16×8) grid points are used for discretization of the velocity space $-4v_{T_i} \leqslant v_\parallel \leqslant 4v_{T_i}$ and $0 \leqslant \mu \leqslant 7B_0/T_{e0}$. The (r,θ,φ) space is discretized with $(128\times 128\times 64)$ points. The safety factor profile is chosen equal to $q(r) = 1 + 2.78(r/a)^{2.8}$ to satisfy $q(r_p) = 1.4$ and $s(r_p) = 0.8$. The results reported on Fig. 1 show that GYSELA simulations are in agreement with the other codes.

5. Collisionless damping of zonal flow and GAM

Rosenbluth and Hinton [10] have shown that linear collisionless processes do not fully damp poloidal flows driven by ITG. The residual level of the zonal flow after the collisionless damping is considered to affect a saturation amplitude of the ITG turbulence. These important observations have lead to another classical test-bed of toroidal gyrokinetic simulations [6,11–13]. In this test an initial electric potential $\hat{\phi}_{00}(t_0,r)$ profile is set in the code and evolves towards a residual flow [14]. This initial state leads to the development of Geodesic Accoustic Modes (GAMs) which are $(m,n) = (0,0)$ modes coupled to sidebands $(m,n) = (\pm 1,0)$ due to the toroidal

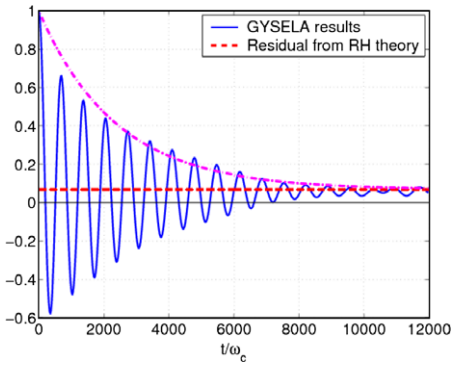

Fig. 3. Time evolution of the zonal flow potential obtained by the GYSELA code (solid line). The dotted horizontal line represents the analytical residual given by [10]. Plot of $\hat{\phi}_{00}(t_0)(1-A_R)\exp(-\gamma_G t)\cos(\gamma_G t) + A_R$ in dashdot line for the expression of γ_G given by [15]. This corresponds in our case to $A_R = 0.0681$ and $\gamma_G = 4.2e-4$.

geometry. These GAMS are Landau-damped because of the finite poloidal wavenumber of the sideband. However there also exist an undamped component $(m,n) = (0,0)$ which corresponds to the ZF. This residual value of ZF has been analytically predicted [14] by: $\hat{\phi}_{00}(t_\infty) = \hat{\phi}_{00}(t_0) \times A_R$ with $A_R = 1/(1 + 1.6q^2/\sqrt{\epsilon})$. As seen in Fig. 3, the residual zonal flow level obtained by GYSELA agrees with the Rosenbluth–Hinton theory. This simulation has been performed with a safety factor profile $q(r)$ equal to $1.5 + 1.5(r/a)^{1.9}$ which corresponds to $q(r_p) = 1.9$. The frequency ω_G and the damping rate γ_G of the GAMS have also been theoretically predicted [12] and more recently by Sugama and Watanabe [15] where the Finite-Orbit-Width effects are taken into account. Fig. 3 shows the behavior of the GAMs simulated by GYSELA in agreement with the predicted decrease $\hat{\phi}_{00}(t)/\hat{\phi}_{00}(t = t_0) = (1 - A_R)\exp(-\gamma_G t)\cos(\gamma_G t) + A_R$.

6. Non-linear simulations

The following non-linear simulations have been performed, for a mesh grid of $(r, \theta, \varphi, v_\parallel, \mu) = (128 \times 128 \times 32 \times 32 \times 16)$, with the same parameters as for the previous linear tests, except for the choice of the density and temperature gradients where the parameters are $\kappa_n = 2.6, \Delta_{r_n} = 1$, $\kappa_T = 12$ and $\Delta_{r_T} = 0.8$. The time step Δt has been chosen equal to $2/\omega_c$. A global simulation of 4000 iterations, as presented in the following, requires around 37 h of CPU time on 32 processors. The turbulence looks fully developed at the end of the simulations we present here, with a broad Fourier spectrum both in m and n. A forthcoming paper will detail the convergence properties of the code. Especially, the saturated regime of turbulence will be explored with regard to the numerical discretization. The first simulation corresponds to a simulation without zonal flow, i.e. the magnetic flux surface average $\langle\phi\rangle$ has been neglected in the quasi-neutrality equation (4). The time evolution of ϕ^2 presented in Fig. 4a exhibits the two expected phases: the linear exponential increase and the non-linear saturation phase. The turbulence relaxation observed in this non-linear phase is due to the relaxation of the profiles. It turns out that the normalized temperature gradient R/L_T drops by approximately 30% between $t = 3000/\omega_c$ and $t = 8000/\omega_c$. Only the temperatures at the boundaries are fixed so that the profile in the center of the simulation domain tends to flatten while the gradients increase in the boundary layer. This point will be improved in the future by developing a flux-driven version of GYSELA namely by driving the system with a constant source. A 3D prototype already exists and yields an intermittent behavior of the temperature gradient [16]. In the present case, the localization of ballooning mode structures at the low field side ($\theta = 0$) is obtained, as seen on the poloidal cross-sections of ϕ plotted in Fig. 4b and c. Adding the zonal flows is not a trivial point. A first important point which has been already highlighted is the fact that the choice of the equilibrium distribution function is crucial. Indeed, as seen on Fig. 5a, taking an equilibrium, which does not depend on the motion invariants only, leads to the development of large scale flows. The final state is dominated by these zonal flows (Fig. 5b) and this takeover arrives early in the simulation (at $t = 500/\omega_c$). At the opposite with an appropriate choice of the equilibrium distribution function the level of ZF is considerably reduced. The simulation shows three phases: the first one with the linear growth of ballooning mode structures (Fig. 6a), the second one shows the distorsion of these radially elongated structures due to the self-generated

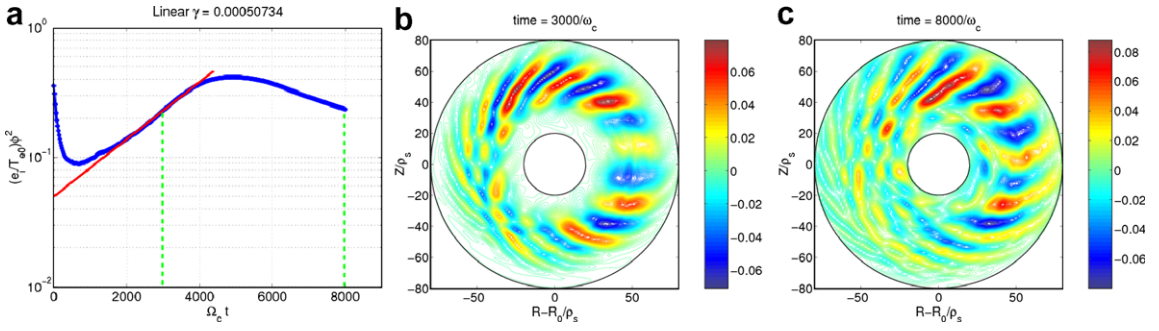

Fig. 4. Simulation where the zonal flows have been artificially suppressed. Time evolution of ϕ^2 in (a). The dotted vertical lines correspond to the times associated to the two poloidal cross-sections of $\phi - \langle\phi\rangle_{\theta,\varphi}$: (b) at the beginning of the saturation phase ($t = 3000/\omega_c$) and (c) at the end of the simulation ($t = 8000/\omega_c$).

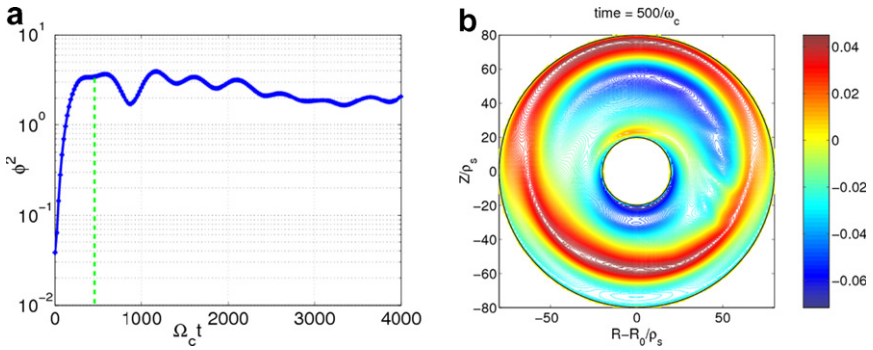

Fig. 5. Simulation with zonal flows and a conventional Maxwellian as initial condition. Time evolution of ϕ^2 in (a). As seen on (b) at time $t = 500/\omega_c$, the poloidal cross-section of $\phi - \langle\phi\rangle_{\theta,\varphi}$ exhibits dominant zonal flows.

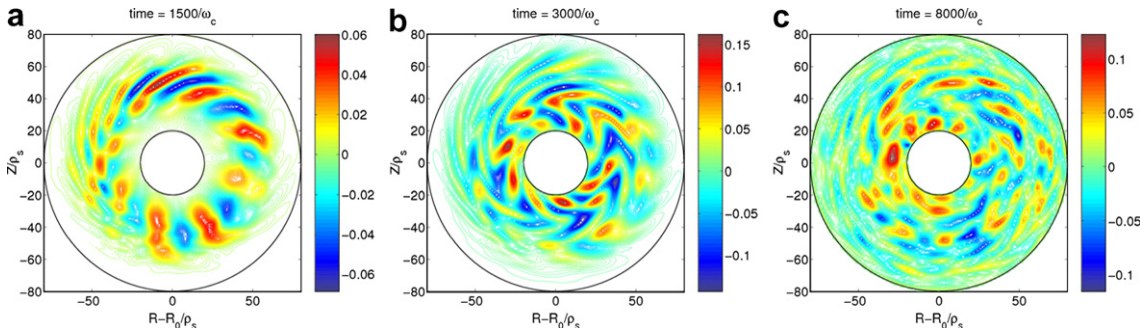

Fig. 6. Simulation with zonal flows and a canonical initial distribution function. Three steps in the evolution are characterized by the poloidal cross-sections of $\phi - \langle\phi\rangle_{\theta,\varphi}$: (b) ballooning mode structure ($t = 1500/\omega_c$), (c) sheared convective cells ($t = 3000/\omega_c$) and turbulent state ($t = 8000/\omega_c$).

zonal flows (Fig. 6b) and the last one characterizes the turbulent regime (Fig. 6c). As suggested by Fig. 6b, the characteristic radial size of the ZF is of the order of a few tens of Larmor radii. In this case, the turbulence saturation is simultaneously governed (*i*) by the profile relaxation, inherent to full-*f* simulations where the equilibrium gradient are allowed to flatten as a result of the turbulent transport, and (*ii*) by the non-linear coupling of the unstable modes. The latter mechanism governs energy cascade processes, possibly leading to the generation of zonal flows.

7. Conclusion

A new 5D global full-*f* gyrokinetic code, named GYSELA, has been developed to study toroidal ITG driven turbulence. The particularity of this code is to use a semi-Lagrangian scheme. The linear growth rates and frequencies agree with the values expected for the reference Cyclone test case. The zonal flows behave as expected in the case of the Rosenbluth–Hinton test. It is found that the decay rate and the oscillation frequency agree with expressions given recently by Sugama and Watanabe [15]. The choice of an equilibrium function which depends only on the motion invariants is crucial to prevent the onset of turbulence due to the development of large scale flows. This problem is solved by defining the initial conditions in terms of a motion invariant, that is chosen so as to depart from the actual minor radius by a small term of order ρ_*.

References

[1] Nevins WM et al. Discrete particle noise in particle-in-cell simulation of plasma microturbulence. Phys Plasmas 2005;12(122305).
[2] Allfrey S et al. A revised delta *f* algorithm for nonlinear pic simulations. Comput Phys Commun 2002;154(2):898–912.

[3] Sonnendrucker E, Roche J. The semi-Lagrangian method for the numerical resolution of Vlasov equation. J Comput Phys 1999;149:201–20.
[4] Grandgirard V et al. A drift-kinetic semi-Lagrangian 4d code for ion turbulence simulation. J Comput Phys 2006;217(2):395–423.
[5] Sarazin Y et al. Interplay between transport barriers and density gradient. Phys Plasmas 2006;13(092307).
[6] Idomura Y et al. Global gyrokinetic simulation of ion temperature gradient driven turbulence in plasmas using a canonical Maxwellian distribution. Nuclear Fusion 2003;43:234.
[7] Angelino P et al. On the definition of a kinetic equilibrium in global gyrokinetic simulations. Phys Plasmas 2006;13:052304.
[8] Dif-Pradalier G et al. Defining an equilibrium state in global full-*f* gyrokinetic models. Commun Nonlinear Sci Numer Simulat 2008:13 (on-line July 2007).
[9] Dimits AM et al. Comparisons and physics basis of tokamak transport models and turbulence simulations. Phys Plasmas 2000;7(3):969–83.
[10] Rosenbluth MN, Hinton FL. Poloidal flow driven by ion-temperature-gradient turbulence in tokamaks. Phys Rev Lett 1998;80(4).
[11] Lin Z et al. Gyrokinetic simulations in general geometry and applications to collisional damping of zonal flows. Phys Plasmas 2000;7(5):1857–62.
[12] Candy J, Waltz RE. An Eulerian gyrokinetic-Maxwell solver. J Comput Phys 2003;186(2):545–81.
[13] Watanabe TH, Sugama H. Velocity-space structures of distribution function in toroidal ion temperature gradient turbulence. Nuclear Fusion 2006;46:24–32.
[14] Hinton FL, Rosenbluth RN. Dynamics of axisymmetric $e \times b$ and poloidal flows in tokamaks. Plasma Phys. Control Fusion 1999:41.
[15] Sugama H, Watanabe TH. Collisionless damping of zonal flows in helical systems. Phys Plasmas 2006;13(012501).
[16] Darmet G et al. Intermittency in flux driven kinetic simulations of trapped ion turbulence. Commun. Nonlinear Sci. Numer. Simulat. 2008:13 (on-line July 2007).